Available online at www.sciencedirect.com
SCIENCE DIRECT®
Journal of volcanology and geothermal research
ELSEVIER
Journal of Volcanology and Geothermal Research 143 (2005) 219–235
www.elsevier.com/locate/jvolgeores

Solubility of H_2O in rhyolitic melts at low pressures and a new empirical model for mixed H_2O–CO_2 solubility in rhyolitic melts

Yang Liu[a,*], Youxue Zhang[a], Harald Behrens[b]

[a]*Department of Geological Sciences, University of Michigan, Ann Arbor, MI 48109-1063, USA*
[b]*Institut für Mineralogie, Universität Hannover, Callinstr. 3, Hannover 30167, Germany*

Received 2 April 2004; accepted 1 September 2004

Abstract

Experiments of H_2O solubility in synthetic haplogranitic and natural rhyolitic melts were conducted at 700–1200 °C and 0.098–25 MPa. Attainment of equilibrium was proven by reversals using starting materials with different initial H_2O contents. Dissolved H_2O contents were determined using Fourier transform infrared spectroscopy. When temperature decreases from 1000 to 700 °C, the solubility of H_2O increases from 0.100 to 0.124 wt.% at 0.098 MPa, from 0.99 to 1.36 wt.% at 11 MPa, and from 1.46 to 2.17 wt.% at 25 MPa. At 6 MPa, the solubility of H_2O increases from 0.63 to 0.77 wt.% from 1200 to 850 °C. Combining our data with those from the literature on pure H_2O and pure CO_2 solubility, mixed H_2O–CO_2 solubility, and H_2O solubility for H_2O–H_2 gas mixture (240 measurements for H_2O and 59 points for CO_2), we develop a single empirical model for solubility of pure H_2O vapor, that of pure CO_2 vapor, as well as that of mixed H_2O–CO_2 vapor in metaluminous high-silica rhyolitic melt. This model applies to the conditions of 700–1200 °C and 0–500 MPa, and consists of two equations:

$$H_2O_t = \left(354.94P_w^{0.5} + 9.623P_w - 1.5223P_w^{1.5}\right)/T + 0.0012439P_w^{1.5} + P_{CO_2}\left(-1.084\times10^{-4}P_w^{0.5} - 1.362\times10^{-5}P_w\right)$$

$$CO_2 = P_{CO_2}(5668 - 55.99P_w)/T + P_{CO_2}\left(0.4133P_w^{0.5} + 2.041\times10^{-3}P_w^{1.5}\right)$$

where H_2O_t is total dissolved H_2O content in wt.%, CO_2 content is in ppm by mass, and T is temperature in Kelvin, $P_w = X_w^f P$ and $P_{CO_2} = X_{CO_2}^f P$ (in MPa), where X_w^f and $X_{CO_2}^f$ are the mole fraction of water and CO_2 in the fluid. The 2σ relative uncertainty is 15% for the H_2O equation, and 20% for the CO_2 equation. The above H_2O equation also applies to H_2O solubility in mixed H_2O–H_2 fluid for $X_{H_2}^f < 0.54$ at 100 MPa, for $X_{H_2}^f < 0.49$ at 200 MPa, and $X_{H_2}^f \leq 0.44$ at 300 MPa (that is, the presence of H_2 in the fluid insignificantly affects H_2O solubility). This empirical model is recommended for the modeling of explosive volcanic eruptions and magma chamber dynamics.

Keywords: H_2O solubility; H_2O–CO_2 solubility; solubility model; exsolution enthalpy; volcanic eruption; metaluminous rhyolite

* Corresponding author. Department of Geophysical Sciences, University of Chicago, Chicago, IL 60637, USA. Tel.: +1 773 834 9719; fax: +1 773 702 9505.
E-mail address: yangl@geosci.uchicago.edu (Y. Liu).

0377-0273/$ - see front matter © 2005 Elsevier B.V. All rights reserved.
doi:10.1016/j.jvolgeores.2004.09.019

1. Introduction

Dissolved volatiles in terrestrial magmas, mainly H_2O and CO_2, power explosive volcanic eruptions. The understanding of the solubility of these volatiles is critical in the modeling of volcanic eruptions. First, the exsolution of these volatiles from magmas in the form of bubbles determines the styles of volcanic eruption (Wilson, 1980). Second, the accurate prediction of other controlling parameters such as melt viscosity, volatile diffusivity, and melt density, in the modeling of volcanic eruptions also depends on the model of volatile solubility. Using the numerical model constrained by experimental bubble growth data (Liu and Zhang, 2000) to evaluate the effect of each physical parameter (such as viscosity and solubility) on bubble growth, Blower et al. (2001) concluded that H_2O solubility at low pressures is critical in the modeling of bubble growth.

The study of H_2O solubility at low pressure is still limited although many experimental studies of H_2O solubility in natural rhyolitic melt or its synthetic analogs (haplogranite) have been undertaken (Goranson, 1931; Burnham and Jahns, 1962; Friedman et al., 1963; Kadik et al., 1972; Khitarov and Kadik, 1973; Shaw, 1974; Dingwell et al., 1984; 1997; Silver et al., 1990; Ihinger, 1991; Holtz et al., 1992, 1995; Blank et al., 1993; Moore et al., 1995, 1998; Gardner et al., 1999; Schmidt et al., 1999; Yamashita, 1999; Mangan and Sisson, 2000; Behrens and Jantos, 2001; Tamic et al., 2001). Previous experimental data were mostly obtained at 850±50 °C and 50–250 MPa. At pressures <50 MPa, data are mostly at 850 °C and those at other temperatures are sporadic and non-systematic (Fig. 1a). Early studies at low pressure (Goranson, 1931; Friedman et al., 1963) contain large uncertainties in the solubility measurements (as discussed in Ihinger et al., 1994; Zhang, 1999a). Even recent data at P<50 MPa still show large scatters (Fig. 1b).

Due to the absence of solubility data at low pressures, models of H_2O solubility in melts are not well constrained at low pressures. Hence, extrapolated solubilities at low pressures may be very different for various models. For example, at 0.1 MPa and 900 °C, the calculated solubility in rhyolitic or haplogranitic melts is: −0.58 wt.% from Mangan and Sisson (2000), −0.03 wt.% from Gardner et al. (1999), 0.01 wt.% from Papale (1997), 0.07 wt.% from Moore et al. (1998) and Yamashita (1999), 0.10 wt.% from Burnham (1975, 1994), Blank et al. (1993), Zhang (1999a), and Newman and Lowenstern (2002), 1.61 wt.% from Tamic et al. (2001). Solubility models of Gardner et al. (1999), Mangan and Sisson (2000), and Tamic et al. (2001) are excluded for further discussion because they are not intended for extrapolation to 0.1 MPa. Although these differences (after excluding the results of Gardner et al., 1999; Mangan and Sisson, 2000; Tamic et al., 2001) appear small, the estimated saturation pressure, which is a significant factor in

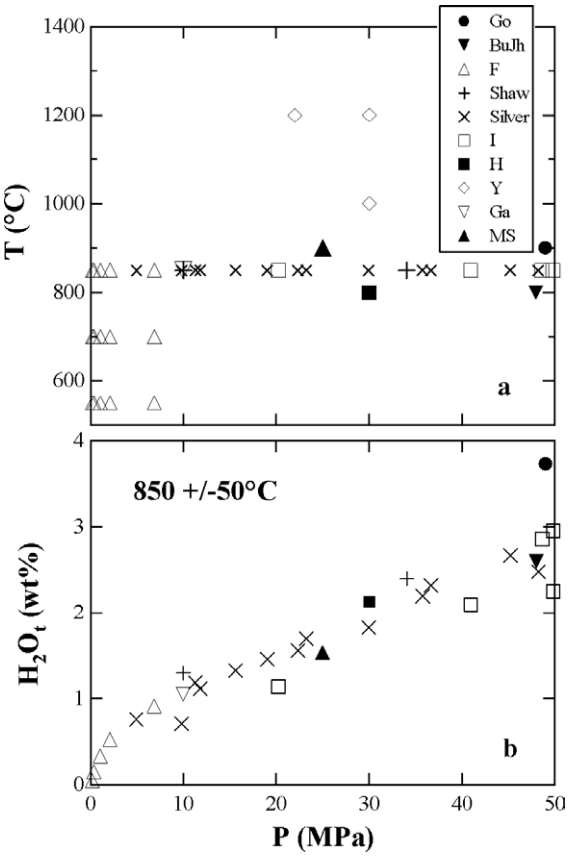

Fig. 1. T and P range of existing experimental data in rhyolitic melts at P<50 MPa (a) and comparison of data at 850 °C (b). Data plotted are: Go, Goranson (1931); BuJh, Burnham and Jahns (1962); F, Friedman et al. (1963); Shaw, Shaw (1974); Silver, Silver et al. (1990); I, Ihinger (1991); H, Holtz et al. (1995); Y, Yamashita (1999); Ga, Gardner et al. (1999); MS, Mangan and Sisson (2000). Data from Goranson (1931) (solid circles) and Ihinger (1991) (open squares) are off the general trend.

determining whether bubbles would grow or not, for a given H_2O content (such as 0.10 wt.%) would differ by a factor of almost 100 (from 0.098 to 8.7 MPa). Furthermore, because viscosity of hydrous melt strongly depends on H_2O contents at low H_2O content (<1 wt.%), even a small difference in calculated solubility may result in a significant difference in viscosity, and hence in calculated bubble growth rates and volcanic eruption dynamics (Blower et al., 2001). For instance, at 2 MPa and 800 °C, the calculated solubility in rhyolitic melts ranges from 0.23 to 0.64 wt.%, which would result in a difference in viscosity (Zhang et al., 2003) by a factor of 50. In this paper, we report an experimental study of H_2O solubility at 0.098–25 MPa in rhyolitic and haplogranitic melts and construct a new empirical model for H_2O–CO_2 solubility in rhyolitic melt.

For clarity, "water" is used here to describe either liquid water or a water vapor phase, whereas H_2O is used for the H_2O component dissolved in the sample. The H_2O species dissolved in the melt are expressed as H_2O_m for the molecular H_2O and OH for hydroxyl groups. The H_2O_t and $H_2O_{t,i}$ represent the total dissolved H_2O and initial total H_2O contents in the sample, respectively. The $X_{H_2O_t}$, $X_{H_2O_m}$, and X_{OH} are the mole fractions of H_2O_t, H_2O_m, and OH in the melt on a single oxygen basis, respectively, where $X_{H_2O_t}=X_{H_2O_m}+0.5X_{OH}$. $X_{CO_2}^{f}$ and X_w^f are the mole fractions of CO_2 and water in fluid, respectively.

2. Experimental methods

2.1. Experimental design and starting materials

Equilibrium experiments were conducted by hydrating a small piece of sample at high temperature under a constant water vapor pressure until equilibrium was reached. At each temperature and pressure, the experimental duration was designed so that it is significantly longer than the estimated time to reach equilibrium by diffusion using the diffusivity from Zhang et al. (1991) and Zhang and Behrens (2000). The attainment of equilibrium was also assessed by conducting experiments with different durations, and by constructing reversals using two obsidians, one undersaturated in $H_2O_{t,i}$ and the other slightly oversaturated in $H_2O_{t,i}$. The chemical compositions of all starting materials are listed in Table 1. Experimental conditions are listed in Tables 2a,b.

Starting materials included natural metaluminous obsidians and a synthetic haplogranite with a normative composition of Ab_{39} Or_{31} Qz_{30} (AOQ of Holtz et al., 1992, 1995). The starting AOQ sample has been also used in the comprehensive H_2O solubility study of Holtz et al. (1992, 1995) at higher pressures. For experiments at room pressure, two natural obsidians were used for reversal experiments: NRO (from Newberry Volcano, CA) with ~0.10 wt.% $H_2O_{t,i}$, and PD (Panum Dome from Mono Craters, CA) with 0.18–0.26 wt.% $H_2O_{t,i}$ (Table 2a). Both obsidians also contain <1 vol.% of magnetite, zircon and unidentified microlites. Silica glass was also used in experiments at ~0.1 MPa in order to verify water vapor pressure. For two experiments at 6–11 MPa, reversals consisted of an obsidian with ~0.2 wt.% $H_2O_{t,i}$ (GB from Glass Butte, Oregon) and another with 0.5–1.0 wt.% $H_2O_{t,i}$ (7b from Mono Craters, California) (Table 2b). Two obsidians with undersaturated $H_2O_{t,i}$ (GB and one of 7b samples or two 7b samples) were used for other experiments at 6–25 MPa. The GB sample contains ~1 vol.% magnetite (estimated using backscattered electron images) and occasional zircon crystals. The 7b samples contain magnetite, unidentified microlites (1 vol.%), and bubbles (<1 vol.%). The slight compositional difference between GB and 7b, and PD and NRO is not expected to have a significant effect on H_2O solubility (Behrens and Jantos, 2001).

2.2. Experiments at ~0.1 MPa

Experiments at atmospheric pressure were conducted in a horizontal tube furnace. The inner diameter of the glass tube is 22 mm. Distilled water was boiled in a flask sealed at the top using a glass stopper but with a side outlet. Silicone tubing connected the side outlet of the flask to one end of the glass tube of the furnace. Heating tapes were wrapped around the whole path from the side outlet to the glass tube and were kept at T>100 °C. Thus, water vapor did not condense along the path during experiment. The other end of the glass tube was open to the atmosphere through a 4-mm diameter hole in a 24-mm-long rubber stopper. Before the

Table 1
Composition of rhyolitic and haplogranitic melts (wt.%)

Location	Mono Craters, California	Newberry Volcano, California	Mono Craters, California	Glass Butte, Oregon	Synthetic	Error (1σ)
Sample name	PD	NRO	7b[a]	GB	AOQ	
SiO_2	77.19	75.03	76.47	77.24	76.62	0.38
TiO_2	0.06	0.2	0.07	0.07	0.03	0.02
Al_2O_3	12.80	13.42	12.44	12.67	13.53	0.15
FeO_t	0.94	1.46	1.02	0.55	0.02	0.05
MgO	0.03	0.13	0.03	0.05	0.01	0.01
CaO	0.53	0.62	0.53	0.51	0.01	0.03
Na_2O	3.98	4.24	4.18	4.30	4.57	0.26
K_2O	4.65	4.99	4.61	4.13	5.19	0.12
Total	100.36	100.38	99.35	99.52	99.97	
H_2O_t	0.18–0.26	0.101	0.5–1.0	~0.20	0.02	
N	6	7	12	3	8	
Comments[b]	mt+m	mt+m, occ zr	b+m	mt occ zr	b	

The composition of rhyolitic glass was analyzed using a Cameca MBX microprobe with a defocused beam (~6 mm in diameter), 3-nA beam current at 15 kV. The Na content was determined by zero-time extrapolation. Glass compositions are normalized to its anhydrous composition. H_2O_t contents were determined using FTIR spectroscopy and the calibration of Zhang et al. (1997b). *N* is the number of microprobe analyses.

[a] The 7b samples are pyroclasts from site 'bb' in the Mono Craters region (Sieh and Bursik, 1986; Newman et al., 1988). The composition of sample 7b is an average of all 7b samples with different $H_2O_{t,i}$: 7b11 with ~1.0 wt.%, 7b22 with ~1.1 wt.%, 7b32 with ~0.5 wt.%, and 7b33 with ~0.8 wt.%. The initial CO_2 contents are: 7b11 with 45 ppm, 7b22 with 45 ppm, 7b32 with 50 ppm, and 7b33 with 38 ppm. The 7b samples also contain <1 vol.% bubbles.

[b] m, microlite; mt, magnetite; b, bubbles; occ zr, occasional zircon crystals. Microlites and bubbles in all rhyolitic samples are less than 1 vol.%. Bubbles in AOQ samples are about 2 vol.%.

samples were placed at the hotspot, the boiling rate was kept high for about 30 min to flush air out of the tube. Afterwards, the boiling rate was decreased to produce ~100 cc STP vapor per minute. From the diffusion-flow equation (Lasaga, 1998, p. 380), we estimate that the dilution of water vapor in the silica glass tube by air is negligible. The elevation of the experiment site gives an atmospheric pressure of 0.098 MPa. Two to five doubly polished glass samples with a thickness of 80–350 μm (measured with a digital micrometer) were placed side by side in a gold boat lining a silica glass boat and put in the hotspot adjacent to a Pt–Pt_{90} Rh_{10} thermocouple.The temperature gradient was 0.2 °C/mm within ±5 mm of the hot spot. During the experiment, temperature fluctuated by <4 °C. At the end of the experiment, the boat was taken out and quenched in air. At 1000 °C and ~0.1 MPa, the sample vesiculates if $H_2O_{t,i}$ is greater than the equilibrium concentration. Therefore, for 1000 °C experiments, samples were degassed at 850 °C for 1 day before they were brought to 1000 °C.

2.3. Experiments at 6–25 MPa

Experiments at 6–25 MPa were conducted in an internally heated pressure vessel (IHPV) at the University of Hannover. Because argon was the pressure medium in the IHPV, the corresponding water vapor pressure was generated by enclosing water and sample into a sealed Au or Pt capsule. The Pt capsules were used only for experiments at 1200 °C. Small pieces of obsidian glasses were cut from a larger piece and then cleaned with acetone, ethanol and distilled water (in the order as written). New Au and Pt tubes (a wall thickness of 0.2 mm and an inner diameter of 2.8 mm) were cleaned with boiling HCl for ~10 min and subsequently with distilled water. After annealing at high temperature (~800 °C for Au and ~1000 °C for Pt), one end of the tube was welded shut. A desired amount of water (0.94–3.14 mg, Table 2b) was loaded using a micro-syringe before a piece of glass was loaded (2–13 mg, Table 2b). After squeezing flat the part above the sample, the other end of the capsule was welded shut while the capsule was cooled by icy water. Each

Table 2a
Solubility experiments and data at 0.098 MPa

Time (h)	T (°C)	Sample	$H_2O_{t,i}$[a] (wt.%)	d[b] (mm)	H_2O_t[a] (wt.%)	Error[c] 1σ	Comments[d]
1008	552	PD3S3	0.256	0.047	0.186	0.005	reversal
		NRO2D2A7	0.102	0.035	0.180	0.006	reversal
		AOQ2S1	0.023	0.052	0.187	0.005	
403	698	PD2A	0.204	0.086	0.126	0.003	reversal, x (≪1 vol.%)
		NRO2D2A5	0.104	0.083	0.124	0.003	reversal, x (≪1 vol.%)
		AOQ1S4	0.026	0.080	0.119	0.003	
359	750	PDS2-2B	0.178	0.260	0.116	0.001	reversal, x (<1 vol.%)
		NROS2-D	0.101	0.229	0.115	0.001	reversal, x (~1 vol.%)
315	851	PD3S1	0.250	0.236	0.106	0.001	reversal, x (<1 vol.%)
		NRO2D2A2	0.101	0.225	0.106	0.001	reversal, x (brown, only on surf)
		AOQ1S1	0.024	0.202	0.102	0.001	
241	850	PDS2B	0.210	0.203	0.105	0.001	reversal, x (≪1 vol.%)
		NROS2-B	0.101	0.201	0.105	0.001	reversal, x (~1 vol.%)
61	850	PDS2	0.210	0.217	0.104	0.001	reversal
		NROS2	0.101	0.230	0.103	0.001	reversal
301	999	PDS2-2D3	nd	0.321	0.102	0.001	
		NRO2D2A4	0.100	0.234	0.102	0.001	
		AOQ1S2-2	0.025	0.163	0.099	0.001	
192	1000	PDS2-2D2	0.194	0.266	0.099	0.001	
		NRO2D2A1	0.101	0.276	0.100	0.001	
		AOQ1S2	0.025	0.260	0.094	0.001	
191	1000	PDS2-2D	0.192	0.220	0.098	0.001	

[a] $H_2O_{t,i}$ is H_2O content before experiments. H_2O_t is H_2O content after experiments. Both $H_2O_{t,i}$ and H_2O_t were determined using FTIR spectroscopy. NRO and PD were samples used to construct reversals: the former was undersaturated in $H_2O_{t,i}$ and the later was oversaturated at experimental conditions. Note that there were no reversals at 1000 °C because samples were degassed at 850 °C before the experiment.

[b] d is the thickness of sample after experiment.

[c] Errors (in wt.%) are the precision of the FTIR analyses, whereas the accuracy of the data (~6% relative) depends on the absorption coefficient.

[d] x, crystallization of fibrous or acicular crystals occurred and number in parentheses indicates the volume percent.

capsule was 18 to 22 mm long. One capsule housed one sample, but two to four capsules were placed in the pressure vessel for each experiment. To check the sealing of the capsule, it was heated in an oven at 70–110 °C for ~12 h and weighed before experiments. To avoid generating excess pressure in the capsule, the amount of water loaded was calculated to produce vapor that occupied half of the volume of the capsule at a given experimental condition (0.94–3.14 mg, Table 2b). However, the amount of water added was much more than the estimated solubility in the sample.

Experiments were conducted in the IHPV for durations of 22 h to 4 days. Capsules were put into the IHPV side by side with the sample at the bottom. The vessel was brought to the desired temperature with a heating rate of 30 °C/min. The temperature gradient along the capsule was monitored by three sheathed type K thermocouples, about 15 mm apart from each other. Two thermocouples bracketed the position of capsules and controlled the furnace temperature. A third was located at the middle of the capsules and monitored the temperature independently. The top and bottom thermocouples recorded same temperatures, but the middle one was usually different by 0.5–26 °C. Although the temperature gradient along the capsule was large, the sample was still under isothermal conditions because its size was <4 mm, leading to only a small temperature difference (<7°C) along the sample. During the experiments, the temperature reading of each thermocouple fluctuated by ±2 °C. Pressure in the experiments was monitored using two transducers and fluctuated by ±0.2 MPa except for three experiments with ±0.4 MPa (Table 2b). At the end of each experiment, quench was achieved by turning off the power of the furnace. Pressure was kept constant within ±0.2 MPa during quench with an automated gas pump. All capsules were flat after experiments and had a similar weight as that before

experiments, indicating no leakage during the run. Capsules were weighed before slitting open. During slitting, water droplet was observed to come out of most capsules, indicating the presence of liquid water in the capsule. The opened capsules were then dried at 70 °C (usually overnight) or 110 °C (for a few hours), and weighed again. The difference of the weight was taken as the amount of free water in the experiments. In most capsules, the amount of water left after the experiment was about the same as or slightly less than that was loaded (Table 2b), indicating that (i) there was no water leakage during the experiment, and (ii) only small amount of water dissolved in the sample, as expected.

Table 2b
Solubility experiments and data at 6.1–25.2 MPa

Time (h)	T (°C)	P[a] (MPa)	Reversals?	Sample	Ms (mg)	Mw (mg)	Mw,e (mg)	H_2O_t (wt.%)	Error[b] (1σ)	Comments[c]
72	700	11	no	GBsol22	2.21	1.41	1.41	1.39	0.02	x (1 vol.%)
				7b33sol22	3.65	1.5	1.51	n.d.	–	x (mt~3 vol.%)
				7b32sol22	3.03	1.39	0.92	1.37	0.07	x (mt~2 vol.%), ib
				AOQsol22	4.11	1.37	1.35	1.33	0.02	ib, x (<1 vol.%)
48	700	25–24.7 (24.8)	no	GBsol20	4.67	3.11	3.03	2.16	0.03	x (<1 vol.%)
				7b33sol20	2.86	3.05	3.09	n.d.	–	x (mt~3 vol.%)
				AOQsol20	2.76	3.14	3.12	2.18	0.03	ib
72	850	6.1	yes	7b33sol7	3.78	1.55	1.33	*0.77*[d]	0.01	b, x[e] (1 vol.%)
				7b32sol7	5.55	1.66	1.64	0.77	0.01	b[f]
				GBsol7	5.74	1.37	1.36	0.79	0.01	
				AOQsol7	4.71	1.48	1.45	0.76	0.01	x (<1 vol.%)
48	850	11.4	no	7b32sol1	3.62	1.26	1.21	1.11	0.02	b (2 vol.%)[g]
				7b22sol1	6.26	1.22	1.08	*1.12*[d]	0.02	b (5 vol.%)
				AOQsol1	4.97	1.35	1.26	1.07	0.02	
94	850	11.2	no	GBsol19	4.98	1.19	1.05	1.10	0.02	
				7b33sol19	3.65	1.3	1.19	1.11	0.02	
				7b32sol19	3.74	1.19	1.06	1.10	0.02	b[g]
				AOQsol19	3.99	1.19	1.03	1.08	0.02	
49	850	25.5–25.1 (25.1)	no	7b32sol2	3.25	2.78	2.69	1.76	0.03	ib
				7b22sol2	5.94	2.45	n.d.	1.75	0.03	b, x (<1 vol.%)
				AOQsol2	4.77	2.48	2.34	1.78	0.04	ib, x (≪1 vol.%)
48.1	995	6.1	yes	GBsol6	5.7	1.06	1.02	0.71	0.01	rx<1 vol.%
				7b32sol6	10.26	1.35	1.37	0.71	0.01	b[g]
				7b33sol6	8.28	1.26	1.19	0.70	0.01	b[g]
				AOQsol6	5.64	1.41	1.31	0.68	0.01	
24.5	1002	11.6–11.2 (11.2)	no	GBsol4	5.36	1.19	1.14	0.99	0.02	ib, rx (1 vol.%)
				7b11sol4	2.48	1.26	1.24	*1.02*[d]	0.02	b (~10 vol.%)
				AOQsol4	3.67	1.04	1.03	0.99	0.02	
24	1000	25.2	no	7b22sol3	6.77	2.46	2.42	1.55	0.02	ib
				7b32sol3	4.14	2.36	2.31	1.54	0.02	
				AOQsol3	5.4	2.5	2.53	1.56	0.02	
24	1000	25	no	GBsol21	3.3	2.7	2.65	1.57	0.02	
				7b32sol21	3.4	2.71	1.8	1.59	0.02	
				AOQsol21	3.65	2.72	1.62	1.56	0.02	
40	1200	6.1	yes	GBsol16	6.19	1.21	1.2	0.64	0.02	rx (5 zircons)
				7b33sol16	6.59	1.1	1.12	*0.64*[d]	0.02	b
				AOQsol16	5	1.09	1.05	0.61	0.02	
24	1200	11	no	GBsol17	7.33	0.94	1.01	0.89	0.02	
				7b33sol17	4.81	0.99	0.94	0.92	0.02	b[g]
22	1200	25	no	GBsol18	12.25	2.28	2.13	1.44	0.02	
				7b33sol18	2.56	2.47	2.45	1.47	0.02	ib
				AOQsol18	5.07	2.41	2.35	1.48	0.02	

3. Infrared analyses

Samples were analyzed for H_2O_t before and after equilibrium experiments using Fourier transform infrared (FTIR) spectroscopy. Baseline of each FTIR spectrum was fit using a flexicurve.

3.1. FTIR analyses for samples for experiments at 0.098 MPa

Samples before and after experiments were analyzed in the main chamber of a Nicolet 60SX FTIR spectrometer. After experiment, samples were polished to a thickness of ~40 to 320 μm. The thickness of the sample was determined using a digital micrometer. For samples with a thickness of 40–50 μm, it is difficult to measure thickness with the digital micrometer. Instead, the method in Tamic et al. (2001) was used and briefly summarized below. The wavelength of the interference fringes (λ is in cm^{-1}) is a function of the thickness of the sample (d) and the apparent refractive index (n): $\lambda=1/(2dn)$. The n value is the apparent refractive index for the specific beam path due to small divergence of the beam in the sample. The λ value was determined using a region of the spectrum away from any absorption bands. Using samples with a thickness of 100–200 μm, which was measured to ± 1 μm using the micrometer, the n values of rhyolitic glasses are ~1.50 in the near infrared region (6000 to 4000 cm^{-1}). Although n depends on the composition of glass and H_2O_t contents (Long and Friedman, 1968; Church and Johnson, 1980), a constant value of 1.50 was used because H_2O_t in the samples only varied from 0.120 to 0.187 wt.%. Thickness calculated using this method agrees with that determined using the micrometer within 1% relative for samples with a thickness of ~200 μm. Because the uncertainty in λ of the very thin sample is $\ll$1% relative, the uncertainty in the determined thickness of those samples (~50 μm) is about 1% relative.

Round apertures with a diameter of 200–1000 μm were placed between the source and the sample to limit the beam. Since H_2O_t contents are low in samples equilibrated at ~0.1 MPa, the absorption band at ~3570 cm^{-1} was used. To convert IR band intensity to H_2O concentration, the molar absorptivity of 80 ± 4.9 L mol^{-1} cm^{-1} is used for rhyolitic and AOQ glasses (Leschik et al., 2004). Leschik et al. (2004) found that the absorption coefficient for the 3570 cm^{-1} band decreases with H_2O_t contents. However, we use a constant value because of the narrow range of the H_2O_t contents. Several points in one sample were analyzed to check the homogeneity of the sample and the precision of H_2O_t contents. The difference between H_2O_t contents from different points, as well as from reversal experiments, is taken as the precision of the solubility. The precision on these solubility estimates also includes error in the thickness measurement and peak intensity. The accuracy of H_2O_t contents (~6% relative) depends on the accuracy of the molar absorptivity.

3.2. FTIR analyses for samples for experiments at 6–25 MPa

Samples were analyzed before and after equilibrium experiments in the main chamber of a Perkin-Elmer Spectrum FTIR GX spectrometer. We verified

Notes to Table 2b:

Ms, Mw, Mw,e are mass of sample, water loaded, and water in capsule after experiment, respectively. A balance with a precision of 0.05 mg was used. The temperature gradient was up to 25 °C/15 mm.

[a] Uncertainty in pressure is 0.2 MPa. When the uncertainty exceeds 0.2 MPa, two numbers given correspond to the minimum and maximum pressure, and the pressure used in the modeling is given in parentheses.

[b] Errors (in wt.%) include the precision of the FTIR analyses including difference in H_2O_t contents from different analyses in one sample, error in the thickness measurement and peak intensity.

[c] b, bubbles and number in parentheses represents the volume percent; rx, residue of original crystals; ib, bubbles are close to surface and might be entrapped water fluid; x, crystallization when fibrous or acicular crystals occurred and number in parentheses indicates the volume percent; mt, magnetite.

[d] Because of high number density of bubbles in the sample, the H_2O_t contents in italic font are discarded and not shown in figures.

[e] Acicular crystals close to edges.

[f] Close to one corner bubble density is high (~10 vol.%), while the remaining part contain about 1 vol.% bubbles. The average bubble size is 34 μm.

[g] Regions of 100–200 μm wide can be analyzed using small apertures with a diameter of 50 μm or 76 μm.

that the main chamber analyses using Perkin-Elmer Spectrum FTIR and those using Nicolet FTIR are in agreement within 2% relative. A round aperture with a diameter of 400 μm was used to limit the beam. H_2O_t contents were determined using the 4520 cm^{-1} and 5230 cm^{-1} bands. Since the expected H_2O_t contents are between 0.6 and 2.2 wt.%, the calibration of Zhang et al. (1997b) on FTIR method was used. Several points in one sample were analyzed to check the homogeneity of the sample and the precision of H_2O_t measurements.

4. Results

Twenty-two experiments were carried out for H_2O solubility in rhyolitic and haplogranitic compositions at 550–1200 °C and 0.1–25 MPa (Tables 2a,b, Figs. 2 and 3). H_2O solubility was obtained for 58 samples, among which 22 samples were studied at ~0.1 MPa. At a given temperature and pressure, the solubility of H_2O in two rhyolitic samples (for reversals) agrees with each other and with the AOQ sample within uncertainties (6% relative for ~0.1 MPa and 2% relative for 6–25 MPa). The attainment of equilibrium is essential for the solubility experiments. Three lines of evidence suggest equilibrium was reached during our experiments. First, the experimental duration was long enough for the sample to reach equilibrium by H_2O diffusion. Second, experiments with different durations at the same temperature and pressure (such as at 850 °C, at ~0.1 MPa with 315 h and 241 h, and 6 MPa with 48 h and 94 h) yield similar H_2O_t contents within uncertainties. Third, solubilities for reversal experiments are similar.

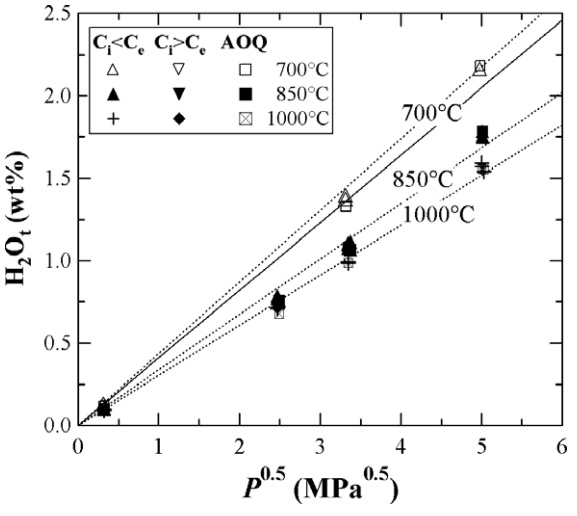

Fig. 2. Dependence of our H_2O solubility data on the square-root of pressure. C_i represents $H_2O_{t,i}$ of the sample, and C_e represents the equilibrium H_2O_t. Dotted lines are linear fits of the data versus $P^{0.5}$. Solid line is calculated using H_2O_t (in wt.%)=$0.4P^{0.5}$, where P is in MPa. Error bars are smaller than the size of the symbols.

Possible experimental problems include crystallization and bubble growth. Because most solubility experiments were carried out below the liquidus temperature of the hydrous rhyolitic melt, the liquid was metastable and crystals may form in the liquid. Furthermore, during experiments, bubbles may form and grow in samples containing excess $H_2O_{t,i}$ and in experiments with oversaturated air and/or CO_2. Whenever there was significant crystal or bubble growth such that no large enough glassy region in the sample can be found to determine H_2O solubility by FTIR, the sample was not used to obtain solubility (italic in Table 2b).

Even though examination with an optical microscope and SEM did not reveal the presence of crystals, the high H_2O concentration in all three samples equilibrated at 550 °C and ~0.1 MPa deviates from the general trend of solubility data (open symbols in Fig. 3a). One possibility for the high "solubility" at 550 °C may be due to temperature below glass transition (glass transition temperature is difficult to define for the isothermal experiment of 42 days). In the glass state, H_2O "solubility" may be controlled by kinetics and by the thermal history of the glass. However, the high "solubility" value is established by reversal experiments, which is more consistent with equilibrium in the melt state than kinetically controlled "solubility" in the glass state. Another possibility is the formation of nanometer-sized hydrous minerals such as biotite, whose peak may be hidden under the ~3570 cm^{-1} band of the glass. In such a case, the measured H_2O content in the glassy sample would be the equilibrium solubility plus the contribution from H_2O in hydrous minerals. To check for such hydrous minerals, TEM studies were carried out on samples equilibrated at 550 °C and no such crystals were positively identified. Although the problem(s) cannot be pinpointed, the

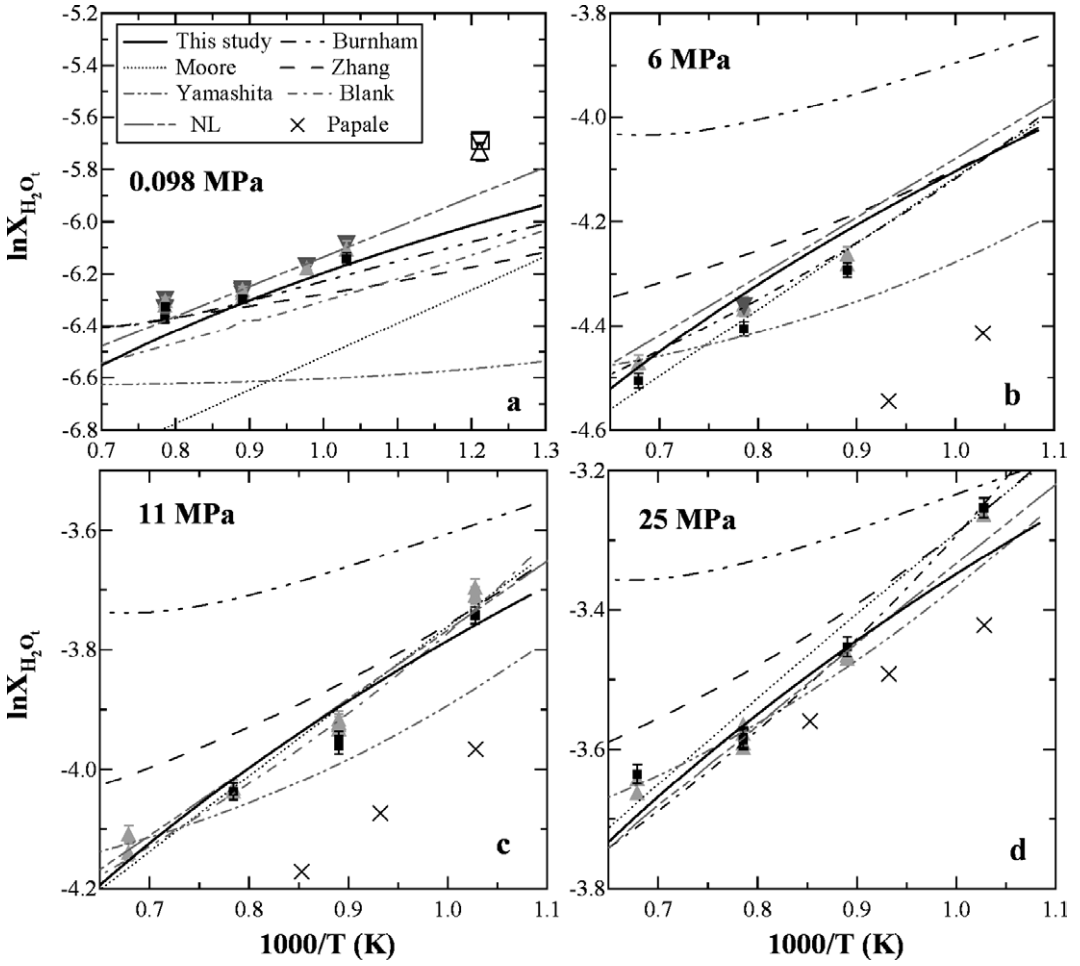

Fig. 3. The temperature dependence of our solubility data and comparison with models. Filled triangles pointing up are rhyolitic samples initially undersaturated with H_2O_t and filled triangles pointing down are those initially oversaturated. Filled squares are H_2O_t contents in AOQ samples. Opened symbols in (a) are results at 550 °C. Error bars are shown if greater than the size of the symbols. Solubility models are plotted in various types of curves. NL indicates the model of Newman and Lowenstern (2002). Note the difference in scales. Solid curves are solubilities calculated using Eq. (2a). Note that the mole fraction of H_2O_t is plotted here whereas Eq. (2a) computes H_2O_t in wt.%.

solubility data at 550 °C and ~0.1 MPa are still problematic and they are excluded hereafter.

Rhyolitic and AOQ samples have similar H_2O solubilities (Figs. 2 and 3) even though their compositions are slightly different. The solubility of H_2O increases with decreasing temperature at low pressures (Figs. 2 and 3). From 1000 to 700 °C, the H_2O_t contents increase by 24% relative at ~0.1 MPa, and by 38% relative at 11–25 MPa (Fig. 3). At a given temperature, the solubility of H_2O is approximately proportional to the square root of pressure (dotted lines in Fig. 2).

5. Discussion

5.1. Exsolution enthalpy at low pressure

Zhang (1999b) proposed a thermodynamic model including H_2O speciation to determine the exsolution enthalpy of H_2O in rhyolitic melts. The dissolution of H_2O is treated by two reactions:

$$H_2O\ (\text{vapor}) \Leftrightarrow H_2O_m\ (\text{melt}) \qquad K_1, \qquad (r1)$$

$$H_2O_m\ (\text{melt}) + O\ (\text{melt}) \Leftrightarrow 2OH\ (\text{melt}) \qquad K_2, \qquad (r2)$$

where O is an anhydrous oxygen (Stolper, 1982a,b). At low H_2O_t (<2.5 wt.%), K_2 is independent of H_2O content, suggesting ideal mixing between H_2O_m, OH and O (Zhang et al., 1997a; Ihinger et al., 1999; Nowak and Behrens, 2001). Hence, equilibrium constants, K_1 and K_2, can be expressed as:

$$K_1 = \frac{X_{H_2O_m}}{f^0_{H_2O}} = A_1 \exp\left(-\frac{\Delta H^0_{r1}}{RT}\right), \quad (1a)$$

$$K_2 = \frac{X^2_{OH}}{X_{H_2O_m} X_O} = A_2 \exp\left(-\frac{\Delta H^0_{r2}}{RT}\right), \quad (1b)$$

where X_i stands for the mole fraction of each species on a single oxygen basis, f_{H_2O} is the fugacity of water vapor calculated from Pitzer and Sterner (1994), A_1 and A_2 are pre-exponential terms, ΔH^0_{r1} and ΔH^0_{r2} are the standard state reaction enthalpy, and the superscript 0 indicates standard state. For the above equations, the standard state for water vapor phase is the hypothetical ideal gas at T and 0.1 MPa, and that for each species in the melt at P and T is the nonexistent hypothetical ideal end member at the activity of 1. Knowing ΔH^0_{r1} and ΔH^0_{r2}, $\Delta \bar{H}_{ex}$ can be calculated using Eq. (16) in Zhang (1999b). Implicit in this theoretical approach is the assumption that mixing between H_2O_m, OH and O is ideal. Below, we use this approach for our low-P solubility data at 0.1–11 MPa.

The reaction enthalpy of reaction (r2), ΔH^0_{r2}, is constrained by the speciation studies (25.9 kJ/mol from Zhang, 1999a; Ihinger et al., 1999; 35.0 kJ/mol from Nowak and Behrens, 2001). Given a speciation model for K_2, we calculate K_1 for each solubility datum. Then, at a given pressure, $\ln K_1$ increases linearly with $1/T$ and the slope of the linear fit gives ΔH^0_{r1}. Although ΔH^0_{r1} depends on the choice of speciation model (either Ihinger et al., 1999; or Nowak and Behrens, 2001), the exsolution enthalpy is roughly independent of the speciation model. The exsolution enthalpy of H_2O at 0.1–11 MPa is small: 13.2–16.5 kJ/mol, indicating the exsolution of H_2O during volcanic eruption does not significantly affect the temperature of rhyolitic melt. For example, complete exsolution of 1 wt.% H_2O from 1 kg of rhyolitic melt will decrease the system temperature by less than 7 °C. Fig. 4 compares exsolution enthalpy obtained from this work (filled circles) with results of

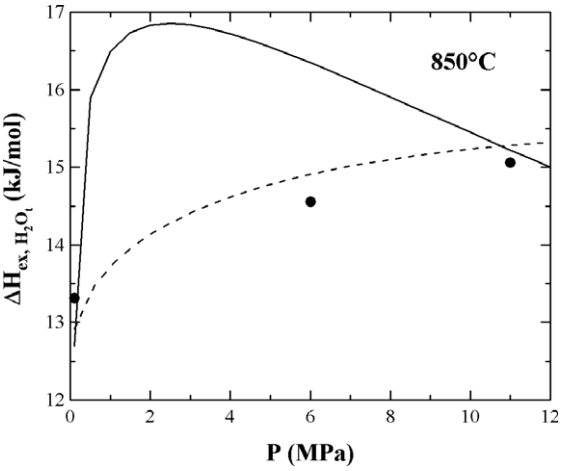

Fig. 4. Exsolution enthalpy of rhyolitic melt at low pressures. Solid curve plots result from Sahagian and Proussevitch (1996). Dashed curve plots result from Zhang (1999b) (note that there is an unknown constant in the results of Zhang, 1999b). Filled circles are results from this work.

Sahagian and Proussevitch (1996) and Zhang (1999b) at 850 °C. Note that Zhang (1999b) only modeled the trend of how exsolution enthalpy depends on pressure but did not obtain the absolute value (that is, there is an unknown constant). When the results of Sahagian and Proussevitch (1996) are compared to our data, the values of exsolution enthalpy are not far off, but as previously pointed out by Zhang (1999b), the trend for the dependence on pressure is off.

5.2. Evaluation of previous models

For estimating H_2O solubility in rhyolite, many empirical and thermodynamic models can be applied (Burnham, 1975, 1994; Blank et al., 1993; Moore et al., 1995, 1998; Yamashita, 1999; Zhang, 1999a; Papale, 1997, 1999; Newman and Lowenstern, 2002). Among these models, three are for H_2O–CO_2 mixtures (Blank et al., 1993; Papale, 1999; Newman and Lowenstern, 2002). Owing to its complexity, we did not evaluate the model of Papale (1999). A square-root equation for pure H_2O solubility, H_2O_t (wt.%)=$0.4P^{0.5}$, P in MPa is often used by volcanologists (e.g. Jaupart and Tait, 1990; Sparks et al., 1994; Navon and Lyakhovsky, 1999) and hence is also included. Below each model is compared with our low-P data (Fig. 3) and then evaluated by comparing with other data (Figs. 5 and 6).

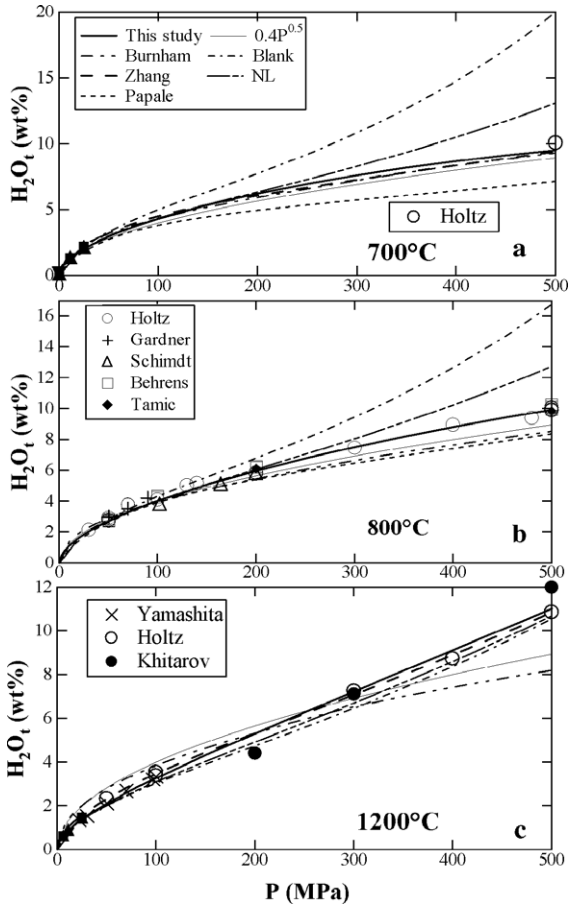

Fig. 5. Comparison of models with experimental data at 700, 800 and 1200 °C. Symbols for solubility data from this study are the same as in Fig. 3. Error bars are smaller than the size of the symbols. Other experimental data are: Khitarov and Kadik (1973), Holtz et al. (1992, 1995), Gardner et al. (1999), Behrens and Jantos (2001), Schmidt et al. (1999), Yamashita (1999), and Tamic et al. (2001).

The often-used square-root equation ($H_2O_t = 0.4P^{0.5}$) fits our low-P solubility data at 700 °C within 10% relative, but misfits by up to 30% relative at higher temperature (Fig. 2). Due to the simplicity of the form, the model also systematical mismatches the experimental data at higher pressures (thin solid line in Fig. 5). For example, at 1200 °C and 100 MPa, the equation overestimates solubility by about 20% relative. Furthermore, this equation is not applicable to mixed H_2O–CO_2 vapor.

The model of Burnham (1975, 1994) overestimates our solubility data by >30% relative at T>850 °C and P>0.1 MPa (long dash-double dotted line in Fig. 3). The model underestimates H_2O solubility at T>700 °C and P>200 MPa (long dash-double dotted line in Fig. 5), with a maximum error of ~35% relative at 1200 °C.

Assuming that the solubility of H_2O and CO_2 with mixed H_2O–CO_2 vapor behaves Henrian, the model of Blank et al. (1993) consists of two equations, one for each gas. The H_2O equation of

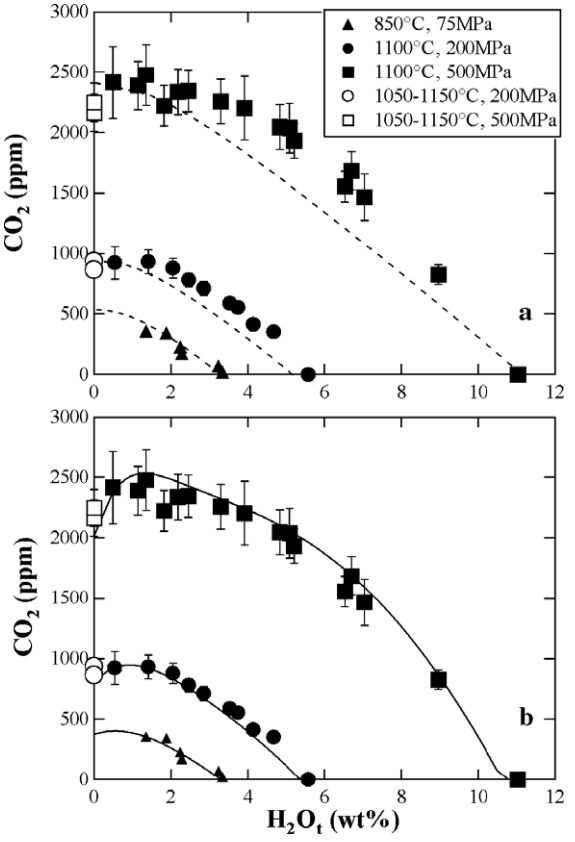

Fig. 6. Comparison of experimental data from Fogel and Rutherford (1990) (open circles and squares), Blank et al. (1993) (filled triangles), and Tamic et al. (2001) (filled circles for filled squares) with (a) the model of Newman and Lowenstern (2002) (dashed curves) and (b) Eq. (2a,b) (solid curves). Error bars are shown if greater than the size of the symbol. Note that $X_w^f + X_{CO_2}^f = 0.98$ for the mixed H_2O–CO_2 fluid in Tamic et al. (2001). In order to show the data of Fogel and Rutherford (1990), CO_2 contents at 200 and 500 MPa are interpolated from the their data at 1050 and 115 °C, respectively. In developing the model (Eq. (2b)), we used raw data.

Blank et al. (1993) fits all data from this study within 15% relative (dash-dotted line in Fig. 3). However, it overestimates H_2O solubility at P>200 MPa by up to a factor of 2 (Fig. 5a). Newman and Lowenstern (2002) improved the H_2O equation using the new experimental results on H_2O speciation in rhyolitic melt (e.g. Zhang, 1999a; Ihinger et al., 1999). For this reason, the model results of Newman and Lowenstern (2002) rather than those of Blank et al. (1993) are shown in Fig. 6.

Papale kindly provided calculated results using the model of Papale (1997) at 700, 800, and 900 °C. At 700 °C, his results are about an order of magnitude smaller at ~0.1 MPa (off scale and hence not shown in Fig. 3a), 10%–30% smaller at 6–25 MPa (crosses in Fig. 3). Compared with other data at higher pressures, the model underestimates experimental data by up to 30% relative at 500 MPa (short dashed curves in Fig. 5a and b).

The model of Moore et al. (1995, 1998) underestimates data at ~0.1 MPa by ~40% relative (dotted lines in Fig. 3), and cannot be applied to calculate H_2O solubility at pressures >300 MPa (Zhang, 1999a).

The model of Yamashita (1999) underestimates our data at ~0.1 MPa by >35% relative (short dash-double dotted curves in Fig. 3), and cannot be applied to calculate H_2O solubility at pressures >200 MPa (Behrens and Jantos, 2001).

The model of Zhang (1999a) underestimates solubility at 700 °C and ~0.1 MPa by ~20% relative and overestimates that at 1200 °C and 6 MPa by ~15% relative (dashed curves in Fig. 3). Although the model of Zhang (1999a) predicts H_2O solubility within 20% relative in a wide pressure and temperature range (dashed curves in Fig. 5), the model is difficult to use in the modeling of eruption dynamics because it requires a complex procedure to calculate water fugacity (Pitzer and Sterner, 1994). Furthermore, the model of Zhang (1999a) is for the solubility of H_2O alone in rhyolitic melt and cannot be applied to mixed H_2O–CO_2 solubilities.

The model of Newman and Lowenstern (2002) predicts all our solubility data within 15% relative, but overestimates the solubility at P>200 MPa (dash-triple dotted curves in Figs. 3 and 5). For example, at 800 °C and 500 MPa, the calculated solubility is ~25% larger than the experimental data (Fig. 5b). The model is also difficult for incorporation in a program to model eruption dynamics. Furthermore, H_2O–CO_2 solubility models of Blank et al. (1993) and Newman and Lowenstern (2002) assume that for H_2O–CO_2 mixture, the solubility of each gas behaves Henrian. The data of Tamic et al. (2001) show that the assumption is not valid at P>200 MPa (Fig. 6).

Accounting for the non-Henrian behavior at high pressures, Behrens et al. (2004b) developed thermodynamic models for CO_2 solubility in rhyolitic and dacitic melt with mixed H_2O–CO_2 vapor, but not for H_2O. Their models also require complex calculations of CO_2 fugacity in mixed H_2O–CO_2 fluids.

Because all previous models suffer from one or more of the following problems: (i) inability to accurately reproduce experimental data; (ii) complexity in solubility calculation; and (iii) invalid assumption of Henrian behavior, there is a need for a new solubility model. Our main focus below is to provide a simple empirical model for mixed H_2O–CO_2 solubility in metaluminous rhyolitic melt, which would also work for pure CO_2 and pure H_2O solubility.

5.3. Solubility data used for the development of the model for mixed H_2O–CO_2 in rhyolitic melt

Table 3 shows the source of data included in the modeling. For H_2O data set, we include solubility data for pure H_2O, mixed H_2O–CO_2 vapor and mixed H_2O–H_2 vapor in both metaluminous high-silica rhyolite and haplogranitic melt, which have identical H_2O solubilities within experimental uncertainties shown by this study (Tables 2a,b, Figs. 2 and 3) and previous studies (e.g. Zhang, 1999a). The whole data set for modeling H_2O solubility in rhyolitic melt with mixed H_2O–CO_2 vapor consists of 240 points (12 points from mixed H_2O–H_2 fluids and 41 points from mixed H_2O–CO_2 fluids) and covers a wide range of temperature (700–1200 °C) and pressure (0.098–500 MPa). The H_2O solubility with mixed H_2O–H_2 in AOQ is included because H_2O and H_2 behave Henrian for $X_{H_2}^{f}$<0.54 at P=100 MPa,

Table 3
Solubility data used for modeling

Source	Melt composition[a]	Fluid phase	T range (°C)	P_t range (MPa)	N
H_2O data					
Khitarov and Kadik (1973)	Granite	H_2O	1200	200–500	3
Shaw (1974)	HSO	H_2O	850	10–200	6
Silver et al. (1990)	HSO	H_2O	850	4.9–200	31
Holtz et al. (1992, 1995)	AOQ	H_2O	700–1350	30–500	46
Blank et al. (1993)	HSO	H_2O–CO_2	850	75	6
Dingwell et al. (1997)	AOQ	H_2O	900	500	1
Gardner et al. (1999)	HSO	H_2O	800–850	10–205	13
Schmidt et al. (1999)	AOQ	H_2O–H_2	950	100–300	12
Yamashita (1999)	HSO	H_2O	850–1200	22–100	15
Behrens and Jantos (2001)	HSO	H_2O	800	50–500	12
Tamic et al. (2001)	HSO	H_2O–CO_2	800, 1100	200, 500	40
This study	HSO	H_2O	700–1200	0.1–25	55
CO_2 data[b]					
Blank et al. (1993)	HSO	H_2O–CO_2	850	75	6
Tamic et al. (2001)	HSO	H_2O–CO_2	800, 1100	200, 500	34
Fogel and Rutherford (1990)	HSO	CO_2	950–1150	101–551	19

[a] Only data in metaluminous high-silica rhyolitic melt (HSO and granite) and haplogranitic melt (AOQ) are used.
[b] All CO_2 data were recalculated using an absorption coefficient of 1214 L mol^{-1} cm^{-1} from Behrens et al. (2004a).

$X_{H_2}^f$<0.49 at P=200 MPa, and $X_{H_2}^f$≤0.44 at P=300 MPa (Schmidt et al., 1999). Measurement of H_2O_t contents may be problematic in the early studies, especially at low H_2O_t. For example, solubility data of Goranson (1931) at 800–900 °C are higher than other studies by 1–2 wt.% (Fig. 1b). Burnham and Jahns (1962) estimated H_2O_t by the presence of surface dimple, which have a precision in the range of ±0.5–1.0 wt.%. Friedman et al. (1963) determined H_2O_t contents (0.1–1.25 wt.%) using the method of weight change, which may be subject to large uncertainties. Therefore, H_2O solubility data of Goranson (1931), Burnham and Jahns (1962), and Friedman et al. (1963) are not included. Data from Dingwell et al. (1984, 1997) on melt compositions other than AOQ are not included. Four outlier points in Silver et al. (1990) are not included in the data set. Data from Ihinger (1991) are excluded owing to the considerable scatter (e.g. 34% relative at 50 MPa and 850 °C, Fig. 1b).

The CO_2 solubility data set (59 points) includes results from Fogel and Rutherford (1990), Blank et al. (1993), and Tamic et al. (2001) (Table 3). We recalculated all CO_2 contents using the absorption coefficient of 1214 L cm^{-1} mol^{-1} (Behrens et al., 2004a). The uncertainty of each datum was also recalculated considering the reported uncertainty in IR absorbance, sample thickness and the absorption coefficient (±87 L cm^{-1} mol^{-1}, Behrens et al., 2004a). Although Pawley et al. (1992) and Tamic et al. (2001) suggest that the fluid phase in the experiments of Fogel and Rutherford (1990) contains unknown amount of CO, we assume it is still pure CO_2 so as to have a large data set to constrain our solubility model. The CO_2 solubility from the study of Kadik et al. (1972) with mixed H_2O–CO_2 fluids is anomalously high compared with recent studies. For example, the CO_2 content (2300 ppm) at 1200 °C and 100 MPa with $X_{CO_2}^f$ of 0.174 by Kadik et al. (1972) is comparable with that by Tamic et al. (2001) at 1100 °C and 500 MPa with $X_{CO_2}^f$ of ~0.7. Hence, we did not include the data of Kadik et al. (1972) in our modeling. One datum (CO_2 of 452 ppm, $X_{CO_2}^f$=0.91) in Blank et al. (1993) with outlier H_2O content (0.51 wt.%) is excluded from both data sets. Solubility data for mixed H_2O–CO_2 fluids from Mangan and Sisson (2000) are not used in both data sets because the fluid composition is not reported.

5.4. Empirical model for mixed H_2O–CO_2 fluids

Based on various considerations and many trial fittings, we choose the following empirical expressions to model H_2O and CO_2 solubility for H_2O–CO_2 mixtures, or pure H_2O, or pure CO_2 solubility in rhyolitic melt:

$$H_2O_t = \left(a_1 P_w^{0.5} + a_2 P_w + a_3 P_w^{1.5}\right)/T + a_4 P_w^{1.5} + P_{CO_2}\left(a_5 P_w^{0.5} + a_6 P_w\right), \quad (2a)$$

$$CO_2 = b_1 P_{CO_2}/T + P_{CO_2}\left(b_2 P_w^{0.5} + b_3 P_w^{1.5}\right) + b_4 P_{CO_2} P_w/T, \quad (2b)$$

where H_2O_t is H_2O content in wt.%, CO_2 content is in ppm by mass, $P_w = X_w^f P$ in MPa, $P_{CO_2} = X_{CO_2}^f P$ (in MPa), and T is temperature in Kelvin. In Eq. (2a), the $P_w^{0.5}$ and P_w terms roughly account for OH and H_2O_m, respectively, while the $P_w^{1.5}$ terms account for the imperfect treatment of OH and H_2O_m species by the first two terms as well as possible complexity due to subspecies (such as AlOH and SiOH) and other species (such as OH pairs and H_3O). Because all experimental data have different uncertainties, we weighted each datum and the calculated pressure terms by the reported uncertainty and then conducted multi-linear regression for Eq. (2a,b) to obtain coefficients a_i and b_i. Fitting parameters and their errors are listed in Table 4. Fig. 6b shows the reproducibility of the model for mixed H_2O–CO_2 solubility data. To calculate pure H_2O or CO_2 solubility, simply let P_{CO_2} in Eq. (2a), or P_w in Eq. (2b) be zero (e.g. Figs. 5 and 7). Eq. (2a) reproduces all experimental H_2O data in the data set within 15% relative except for eleven points. The maximum error for H_2O_t is 28% relative for X_w^f of 0.12 at 1100 °C and 500 MPa. For pure H_2O solubility (187 points), four points have relative error≥15%. The maximum absolute error for H_2O_t is 0.99 wt.% at 1200 °C, 500 MPa, and 12 wt.% H_2O_t (Khitarov and Kadik, 1973). Calculated CO_2 contents using

Table 4
Parameters in Eq. (2a,b)

i	Eq. (2a)		Eq. (2b)	
	a_i	Error	b_i	Error
1	354.94	4.55	5668	127
2	9.623	0.923	0.4133	0.0491
3	−1.5223	0.0722	2.041×10^{-3}	0.285×10^{-3}
4	0.0012439	0.0000499	−55.99	8.36
5	-1.084×10^{-4}	0.406×10^{-4}		
6	-1.362×10^{-5}	0.352×10^{-5}		

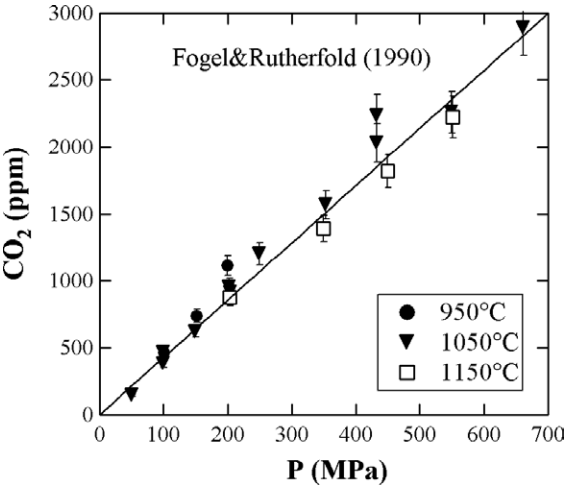

Fig. 7. The fit of Eq. (2b) for CO_2 solubility data at X_w^f=0. The calculation is shown for 1050 °C (solid line). Error bars are shown if greater than the size of the symbol.

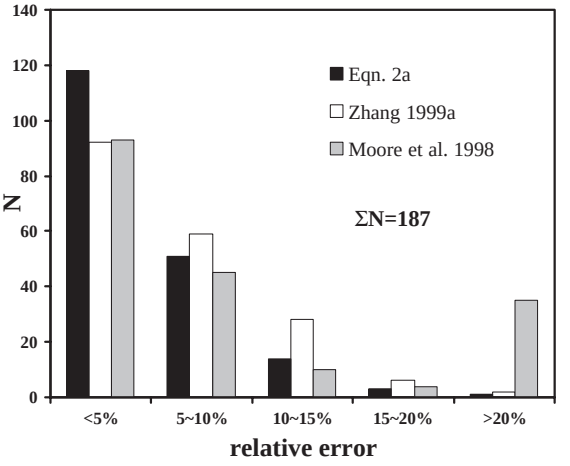

Fig. 8. Histogram of the relative errors of selected models. Only experimental data with pure H_2O fluid are compared here (187 points). The relative error between experimental data and the calculated values is defined as $(C_{cal}-C_{exp})/C_{exp}$.

Eq. (2b) reproduce all experimental data in the CO_2 data set within 15% relative except for six points. The maximum deviation for CO_2 is 47% relative at 1050 °C and 50.4 MPa for pure CO_2 fluid. There are some peculiar features for the solubility data of CO_2 in rhyolitic melt in equilibrium with a mixed CO_2–H_2O fluid. These features are well fit by our empirical model and worth pointing out:

(1) CO_2 solubility in rhyolitic melt in equilibrium with pure CO_2 fluid decreases as temperature increases (Fogel and Rutherford, 1990; Blank et al., 1993), whereas with mixed CO_2–H_2O fluid the solubility increases with increasing temperature at 500 MPa (Tamic et al., 2001).

(2) In some T–P region (such as 500 MPa and 1100 °C), CO_2 solubility decreases with increasing $X^f_{CO_2}$(Fig. 6). For example, according to Fogel and Rutherford (1990), CO_2 solubility at 1100 °C, 500 MPa and $X^f_{CO_2}$=1 is about 2200 ppm (note that their data have been corrected using new molar absorptivity). The data of Tamic et al. (2001) at 1100 °C and 500 MPa show that as $X^f_{CO_2}$ decreases from 1, CO_2 solubility increases to a maximum of 2480 ppm at $X^f_{CO_2}$=0.873 and then decreases. The solubility of CO_2 at $X^f_{CO_2}$=1 is about the same as that at $X^f_{CO_2}$=0.6.

One possible explanation is that the fluid phase in the experiments of Fogel and Rutherford (1990) contain unknown amount of CO (Pawley et al., 1992; Tamic et al., 2001). Assuming these features are real, they would imply that at high pressures (≥200 MPa), dissolution of H_2O increases the equilibrium constant of CO_2 solubility (X_{CO_2}/f_{CO_2}) significantly, whereas at low pressures (such as 75 MPa) CO_2 and H_2O solubilities behave roughly in a Henrian manner (Blank et al., 1993).

The major advantage of our solubility model (Eqs. (2a) and (2b)) is its simplicity. Furthermore, the model does better (sometimes only very slightly, Fig. 8) in fitting the solubility data than the most sophisticated thermodynamic models available. Hence we recommend the use of the model for solubility calculations in metaluminous high-silica rhyolitic melt, especially by the volcanological community. However, because it is empirical, the model application should be restricted to 700–1200 °C and 0–500 MPa, and extrapolation is not encouraged.

Acknowledgments

This study was supported by NSF grants EAR-9972937, EAR-0125506, EAR-0228752. We thank Otto Diedrich for preparation of polished samples after experiments, Sha Zhu and Daming Wang with the help of TEM, and P. Papale for providing calculated solubility using his solubility model. Discussion with Eric Essene was of great help. We would also like to thank M. Rutherford, D. Sahagian, and an anonymous reviewer for their constructive reviews that shaped the final manuscript.

References

Behrens, H., Jantos, N., 2001. The effect of anhydrous composition on water solubility in granitic melts. Am. Mineral. 86, 14–20.

Behrens, H., Tamic, N., Holtz, F., 2004a. Determination of molar absorption coefficient for the IR absorption band of CO_2 in rhyolitic glasses. Am. Mineral. 89, 301–306.

Behrens, H., Ohlhorst, S., Holtz, F., Champenois, M., 2004b. CO_2 solubility in dacitic melts equilibrated with H_2O–CO_2 fluids—implications for modeling the solubility of CO_2 in silicic melts. Geochim. Cosmochim. Acta (revised).

Blank, J.G., Stolper, E.M., Carroll, M.R., 1993. Solubilities of carbon dioxide and water in rhyolitic melt at 850 °C and 750 bars. Earth Planet. Sci. Lett. 119, 27–36.

Blower, J.D., Mader, H.M., Wilson, S.D.R., 2001. Coupling of viscous and diffusive controls on bubble growth during explosive volcanic eruptions. Earth Planet. Sci. Lett. 193, 47–56.

Burnham, C.W., 1975. Water and magma: a mixing model. Geochim. Cosmochim. Acta 39, 1077–1084.

Burnham, C.W., 1994. Development of the Burnham model for prediction of H_2O solubility in magmas. Rev. Mineral. 30, 123–130.

Burnham, C.W., Jahns, R.H., 1962. A method for determining the solubility of water in silicate melts. Am. J. Sci. 260, 721–745.

Church, B.N., Johnson, W.M., 1980. Calculation of the refractive index of silicate glasses from chemical composition. Geol. Soc. Am. Bull. 91, I 619–I 625.

Dingwell, D.B., Harris, D.M., Scarfe, C.M., 1984. The solubility of H_2O in melts in the system SiO_2–Al_2O_3–Na_2O–K_2O at 1 to 2 kbars. J. Geol. 92, 387–395.

Dingwell, D.B., Holtz, F., Behrens, H., 1997. The solubility of H_2O in peralkaline and peraluminous granitic melts. Am. Mineral. 82, 434–437.

Fogel, R.A., Rutherford, M.J., 1990. The solubility of carbon dioxide in rhyolitic melts: a quantitative FTIR study. Am. Mineral. 75, 1311–1326.

Friedman, I., Long, W., Smith, R., 1963. Viscosity and water content of rhyolitic glass. J. Geophys. Res. 68, 6523–6535.

Gardner, J.E., Hilton, M., Carroll, M.R., 1999. Experimental constrains on degassing of magma: isothermal bubble growth during continuous decompression from high pressure. Earth Planet. Sci. Lett. 168, 201–218.

Goranson, R.W., 1931. The solubility of water in granite magmas. Am. J. Sci. 22, 481–502.

Holtz, F., Behrens, H., Dingwell, D.B., Taylor, R.P., 1992. Water solubility in aluminosilicate melts of haplogranite composition at 2 kbar. Chem. Geol. 96, 289–302.

Holtz, F., Behrens, H., Dingwell, D.B., Johannes, W., 1995. H_2O solubility in haplogranitic melts: compositional, pressure, and temperature dependence. Am. Mineral. 80, 94–108.

Ihinger, P.D., 1991. An experimental study of the interaction of water with granitic melts. PhD dissertation, California Inst. Technology, Pasedena, CA.

Ihinger, P.D., Hervig, R.L., McMillan, P.F., 1994. Analytical methods for volatiles in glasses. Rev. Mineral. 30, 67–121.

Ihinger, P.D., Zhang, Y., Stolper, E.M., 1999. The speciation of dissolved water in rhyolitic melt. Geochim. Cosmochim. Acta 63, 3567–3578.

Jaupart, C., Tait, S., 1990. Dynamics of eruptive phenomena. Rev. Mineral. 24, 213–238.

Kadik, A.A., Lukanin, O.A., Lebedev, Ye.B., Korovushkina, E.Ye., 1972. Solubility of H_2O and CO_2 in granite and basalt melts at high pressures. Geochem. Int. 9, 1041–1050.

Khitarov, N.I., Kadik, A.A., 1973. Water and carbon dioxide in magmatic melts and peculiarities of the melting process. Contrib. Mineral. Petrol. 41, 205–215.

Lasaga, A.C., 1998. Kinetic Theory in the Earth Science. Princeton University Press, Princeton, NJ, p. 811.

Leschik, M., Heide, G., Frischat, G.-H., Behrens, H., Wiedenbeck, M., Wagner, N., Heide, K., Geiβler, H., Reinholz, U., 2004. Determination of H_2O and D_2O contents in rhyolitic glasses using KFT, NRA, EGA, IR spectroscopy, and SIMS. Phys. Chem. Glasses 45, 238–251.

Liu, Y., Zhang, Y., 2000. Bubble growth in rhyolitic melt. Earth Planet. Sci. Lett. 181, 251–264.

Long, W., Friedman, I., 1968. The refractive index of experimentally hydrated rhyolite glass. Am. Mineral. 53, 1754–1756.

Mangan, M., Sisson, T., 2000. Delayed, disequilibrium degassing in rhyolite magma: decompression experiments and implications for explosive volcanism. Earth Planet. Sci. Lett. 183, 441–455.

Moore, G., Vennemann, T., Carmichael, I.S.E., 1995. Solubility of water in magmas to 2 kbar. Geology 23, 1099–1102.

Moore, G., Vennemann, T., Carmichael, I.S.E., 1998. An empirical model for the solubility of H_2O in magmas to 3 kilobars. Am. Mineral. 83, 36–42.

Navon, O., Lyakhovsky, V., 1999. Vesiculation processes in silicic magmas. In: Gilbert, J.S., Sparks, R.S.J. (Eds.), The physics of explosive volcanic eruptions 145, pp. 27–50.

Newman, S., Lowenstern, J.B., 2002. VOLATILECALC: a silicate melt-H_2O–CO_2 solution model written in visual basic for excel. Comput. Geosci. 28, 597–604.

Newman, S., Epstein, S., Stolper, E.M., 1988. Water, carbon dioxide, and hydrogen isotopes in glasses from the ca 1340 AD eruption of the Mono Craters, California—constraints on degassing phenomena and initial volatile content. J. Volcanol. Geotherm. Res. 35, 75–96.

Nowak, M., Behrens, H., 2001. Water in magmas: a slippery problem gets more grip. Earth Planet. Sci. Lett. 184, 515–522.

Papale, P., 1997. Modeling of the solubility of a one-component H_2O or CO_2 fluid in silicate liquids. Contrib. Mineral. Petrol. 126, 237–251.

Papale, P., 1999. Modeling of the solubility of a two-component H_2O+CO_2 fluid in silicate liquids. Am. Mineral. 84, 477–492.

Pawley, A.R., Holloway, J.R., McMillan, P.F., 1992. The effect of oxygen fugacity on the solubility of carbon–oxygen fluids in basaltic melt. Earth Planet. Sci. Lett. 110, 213–225.

Pitzer, K.S., Sterner, S.M., 1994. Equation of state valid continuously from zero to extreme pressures for H_2O and CO_2. J. Chem. Phys. 101, 3111–3116.

Sahagian, D.L., Proussevitch, A.A., 1996. Thermal effects of magma degassing. J. Volcanol. Geotherm. Res. 74, 19–38.

Schmidt, B.C., Holtz, F., Pichavant, M., 1999. Water solubility in haplogranitic melts coexisting with H_2O–H_2 fluids. Contrib. Mineral. Petrol. 136, 213–224.

Shaw, H.R., 1974. Diffusion of H_2O in granitic liquids, I, experimental data, and II, mass transfer in magma chambers, in Geochem. In: Hofmann, A.W., et al., (Eds.), Transport and Kinetics. Carnegie Inst. of Wash., Washington, D.C, pp. 139–170.

Sieh, K., Bursik, M., 1986. Most recent eruptions of the mono craters, eastern central California. J. Geophys. Res. 91, 12539–12571.

Silver, L.A., Ihinger, P.D., Stolper, E.M., 1990. The influence of bulk composition on the speciation of water in silicate glasses. Contrib. Mineral. Petrol. 104, 142–162.

Sparks, R.S.J., Barclay, J., Jaupart, C., Mader, H.M., Phillips, J.C., 1994. Physical aspects of magma degassing I. Experimental and theoretical constraints on vesiculation. Rev. Mineral. 30, 413–445.

Stolper, E.M., 1982a. Water in silicate glasses: an infrared spectroscopic study. Contrib. Mineral. Petrol. 81, 1–17.

Stolper, E.M., 1982b. The speciation of water in silicate melts. Geochim. Cosmochim. Acta 46, 2609–2620.

Tamic, N., Behrens, H., Holtz, F., 2001. The solubility of H_2O and CO_2 in rhyolitic melts in equilibrium with a mixed CO_2–H_2O fluid phase. Chem. Geol. 174, 333–347.

Wilson, L., 1980. Relationships between pressure, volatile content and ejecta velocity in three types of volcanic explosions. J. Volcanol. Geotherm. Res. 8, 297–313.

Yamashita, S., 1999. Experimental study of the effect of temperature on water solubility in natural rhyolite melt to 100 MPa. J. Petrol. 40, 1497–1507.

Zhang, Y., 1999a. H_2O in rhyolitic glasses and melts: measurement, speciation, solubility, and diffusion. Rev. Geophys. 37, 493–516.

Zhang, Y., 1999b. Exsolution enthalpy of water from silicate liquids. J. Volcanol. Geotherm. Res. 88, 201–207.

Zhang, Y., Behrens, H., 2000. H_2O diffusion in rhyolitic melts and glasses. Chem. Geol. 169, 243–262.

Zhang, Y., Stolper, E.M., Wasserburg, G.J., 1991. Diffusion of water in rhyolitic glasses. Geochim. Cosmochim. Acta 55, 441–456.

Zhang, Y., Jenkins, J., Xu, Z., 1997a. Kinetics of the reaction $H_2O+O=2OH$ in rhyolitic glasses upon cooling: geospeedometry and comparison with glass transition. Geochim. Cosmochim. Acta 61, 2167–2173.

Zhang, Y., Belcher, R., Ihinger, P.D., Wang, L., Xu, Z., Newman, S., 1997b. New calibration of infrared measurement of dissolved water in rhyolitic glasses. Geochim. Cosmochim. Acta 61, 3089–3100.

Zhang, Y., Xu, Z., Liu, Y., 2003. Viscosity of hydrous rhyolitic melts inferred from kinetic experiments, and a new viscosity model. Am. Mineral. 88, 1741–1752.